FATIGUE IN WELDED TUBULAR JOINTS

A. Abel

School of Civil and Mining Engineering,
The University of Sydney, N.S.W. 2006, Australia

Third International Conference on Biaxial/Multiaxial Fatigue,
April 3-6, 1989, Stuttgart, FRG

ABSTRACT

A typical offshore steel platform structure may contain hundreds of welded tubular joints, the fatigue of which is a main concern in the design as well as during the operational life of the platform. Because of the geometries involved - a cylinder bisected by another cylinder for load transfer purposes - all three loading modes (axial, in-plane bending and out-of-plane bending separately and in any combination) will result in a biaxial stress state in the vicinity of the weld-line where fatigue is taking place.

Experimental and Finite Element Methods were used to evaluate the existing stress states by determining the so-called stress and strain concentration factors, SCF and SNCF respectively, for a number of large full-scale tubular joints. Following this, the crack initiation and crack propagational characteristics were studied in both the as-welded and stress relieved conditions. The results are presented with reference to the biaxial stress states existing in the vicinity of the weld lines.

INTRODUCTION

The advantages offered by tubular joints in onshore applications, such as warehouses, factory buildings, space frames, tower structures, bridges, etc. may be measured in terms of economy, depending on the skill of both designers and fabricators. In the case of offshore, two additional advantages are offered when circular tubular members are used. One relates to the drag characteristics, and the other to buoyancy during the installation procedure. As a result of these and other considerations, tubular structures have dominated offshore development since the early 1970s.

In general, the joints in tubular structures are referred to as nodes, and these are made up by welding brace members to the continuous unperforated chords; this results in geometrical configurations which resemble letters of the alphabet: T, K, Y, etc. In offshore structures, nodes with more than ten brace members intersecting a single chord are not uncommon (1). The local maximum stress in a joint is the so-called 'hot-spot' stress, the magnitude of which is made up from (a) applied nominal stress, (b) geometrical stress (associated with the load transfer characteristics between the tubulars) and (c) notch stresses (which are particularly influenced by the weld detail). These two latter may be envisaged by referring to Fig. 1.

When fatigue in offshore applications is considered, two additional aspects must be taken into account: residual stresses and wave direction distribution. It is generally assumed that in the neighbourhood of a weld, yield strength magnitude residual stresses are present, irrespective of the strength of the parent metal of the tubulars. The distribution of loading waves, in respect of direction and height, introduces some additional complexities (Fig. 2).

As a consequence of wave direction distribution, the loading which may take place in practice is axial, in-plane bending, out-of-plane bending, independently or in any

combination of these - all of which introduce biaxiality as shown in Figs 3 - 4.

A programme of research relevant to fatigue in steel offshore structures has been completed, and some of the details of this investigation are presented below.

OUTLINE OF THE TESTS

Nine large, full-scale specimens were fatigue tested in the as-welded or stress relieved states, as shown in Table 1. The plate material was originally developed for the fabrication of tubulars to be used in the construction of the Mackerel, Tuna and Snapper oil platforms located in the Bass Strait off the south-east coast of Australia. Specimens 2, 5, 7 and 9 were subjected to post-weld heat treatment, subsequent to the brace to chord welding, to relieve residual stresses. This was done in accordance with Australian Standard AS1958-1976, 'SAA Submarine Pipeline Code', which specifies a heating rate of 100°C/h, a holding time at 590°C - 620°C for one hour per 25 mm wall thickness, followed by cooling at 150°C/h to 300°C, finally ending by cooling in still air.

Comprehensive strain gauging was used, including single element, rosette, and crack propagation gauges, as illustrated in Fig. 5. Gauges were positioned on the outside and inside surfaces for both brace and chord. Two systems were used to monitor gauge response: a 200 channel Hewlett Packard automatic data acquisition, and a 200 channel Intercole Systems Compulog. A number of utility computer programs (FORTRAN) were written to process the data into more meaningful form.

A specially designed loading rig allowed the simultaneous operation of three hydraulic jacks. The combination of jacks provided a dynamic capacity of -50 to +50 tonnes operated by a servo-hydraulic Amsler P960 pulsator, an accumulator, and a dynamometer system. The specimens were bolted in place by flanges welded to the ends of the tubes.

Finite element methods (FEM) were also used to determine SCFs. While many element types are available to analyse shell structures, as in tubular joint intersections, Irons and Ahmad's isoparametric semi-loof shell and beam elements were found to be the most appropriate to determine the location and magnitude of hot-spot stresses (5, 6). The shell element is based on thin shell assumptions, in which each tubular member is represented by a cylindrical surface at the mid-thickness. This leads to some difficulties when results are compared with those obtained by experimental methods, as shown in Fig. 6.

RESULTS

A. Static Response

Testing commenced with incremental static loading, which allowed the determination of the load transfer characteristics and stress and strain concentration factors: SCF and SNCF respectively. The biaxial stress states are illustrated by Fig. 7 for the T type specimen, and by Figs 8 - 10 for the TK specimen.

Experimentally determined SCFs and SNCFs are presented in Figs 11 - 12 and in Table 2. The differences between SCFs and SNCFs are attributed to the existing biaxial stress states. Using only single element gauges to determine SCFs, the values were up to 20% higher than those of the SNCFs relying on the data obtained from the rosette gauges.

B. Finite Element Results

The biaxiality is greatly influenced by the geometries of the tubulars involved, and thus the SCFs are also affected. The FEM of analysis predicted the SCFs with reasonable accuracy, as shown in Fig. 13, while the influence of tubular geometries is illustrated by Figs 14 - 15.

C.   Fatigue Behaviour

The fatigue results obtained on the nine specimens with the application of thirteen loading programmes, are presented in Table 3 and shown against recommended design curves in Fig. 16. There are four aspects: fatigue rack initiation, N_i; through thickness propagation, N_t; cycles to failure, N_f; and stress relieving, which are detailed below.

Crack initiation numbers were determined through strain gauge signals, as indicated in Fig. 17. Biaxiality in loading persists till a through thickness crack develops, Fig. 18. Through thickness penetration was determined by hydrogen leak detection. This was made possible by filling the chord, before testing, with a low concentration of hydrogen under very low pressure. After sealing and monitoring the test piece during fatigue with a 'Figaro' gas sensor, the leaking of hydrogen could be detected. Thus the through thickness fatigue life determination can be considered as quite accurate. Typical crack initiation, propagation and penetration details are presented in Figs 19 - 21.

As Fig. 16 shows, there is a significant increase in fatigue life as a result of stress relieving. These results should be viewed against the fact that cycling took place not only with R = -1, but with R tending to zero (Fig. 22) and, equally important, that the parent material showed a decrease in fatigue performance as a result of stress relieving, Fig. 23.

CONCLUSIONS

A number of conclusions can be drawn from the above work, some of which are presented below.

1.   In welded tubular offshore steel platforms, loading in the axial, in-plane bending, and out-of-plane bending modes, separately or in any combination, leads to biaxial stress states.

2. The biaxial response persists during fatigue crack propagation in the vicinity of the crack until through thickness crack penetration takes place.

3. Multiple crack initiation took place, leading to crack coalescence and a strong sideways propagation.

4. Surface cracking along the brace-chord weld-line of the TK specimen reached a length of the order of 1400 mm before penetrating the 20 mm thickness of the plate material.

5. Stress relieving improved the fatigue performance with respect to crack initiation, crack propagation and cycles to failure.

ACKNOWLEDGMENTS

REFERENCES

1. Gurney, T.R., 'Fatigue of Welded Structures', 2nd edn, Cambridge University Press, 1979.

2. Wintermark, H., Fabrication and Control of the Fatigue and Brittle Fracture Risk, IIW Conference, Sydney, 1976, Lecture 17.

3.   Ir D. Zijp, Spectral Dynamic Fatigue Analysis of the 'Andoc Dunlin A' Platform, International Conference on Environmental Forces on Engineering Structures, London, July 1979, Pentech Press.

4.   Yura, J., Zettlemoyer, N., and Edwards, I.F., J. Struct. Div., ASCE, Vol. 107, No. ST10, Oct. 1981.

5.   Irons, B.M., 'The Semiloof Shell Element', Chapter 11, Finite Elements for Thin Shells and Curved Membranes, Eds D.G. Ashwell and R.H. Gallagher, Wiley 1976, pp 197-222.

6.   Irons, B.M. and Ahmad, S., 'Techniques of Finite Element', 2nd edn, Ellis Horwood Ltd, John Wiley & Sons, 1980.
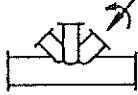
Table 1   Specimen Details

T type
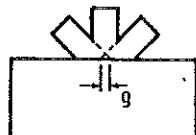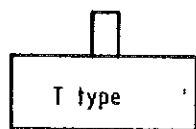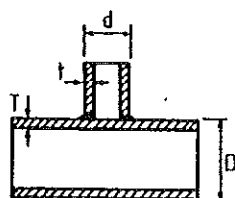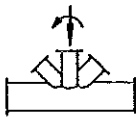
TK type

Spec. No. and Type		Condition AW; SR[1]	Dimensions in mm				Dimensional Parameters				
			D	T	d	t	α; L/R	β; t/R	γ; R/T	τ; t/T	ζ; g/d
1	T	AW	610	19.7	406	9.7	7.26	0.67	15.0	0.49	
2	T	SR	610	19.7	406	9.7	7.26	0.67	15.0	0.49	
3	T	AW	610	12.3	406	9.7	7.17	0.66	24.3	0.79	
4	T	AW	508	19.4	406	9.7	8.43	0.81	12.6	0.50	
5	T	SR	508	19.4	406	9.7	8.43	0.81	12.6	0.50	
6	T	AW	490	15.0	267	10.0	8.74	0.54	15.4	0.665	
7	T	SR	490	15.0	267	10.0	8.74	0.54	15.4	0.665	
8	TK	AW	710	20.3	456	16.5	15.4	0.638	17.0	0.81	
9	TK	SR	710	20.3	456	16.5	15.4	0.638	17.0	0.81	-0.43

T Steel : 0.18 C , 1.58 Mn , 0.41 CEQ

TK Steel : 0.12 C , 0.94 Mn , 0.28 CEQ

1. AW = as welded, SR = stress relieved

Table 2   SCF/SNCF for Axial Loading, Out-of-Plane and In-Plane Bending

LOADING CONFIGURATIONS	A. AXIAL LOADING SADDLE (C) CROWN (N)		B. IN-PLANE BENDING CROWN (S) CROWN (N)		C. OUT-OF-PLANE BENDING SADDLE (C) SADDLE (N)	
	-8.38 (1) -10.06 (2)	-4.30 -4.65	1.56** 1.83**	0.52 0.58	4.74 5.29	4.00 4.48
	-5.15 3.93 (3.05)* -6.20 4.35 (3.29)*		-0.18 -0.19	1.56 1.83	2.74 3.07	3.40 3.80
	-10.30 -12.40	-6.98 -7.64	-2.04 -2.39	-2.04 -2.39	5.58 6.31	6.16 6.96
	0.00 0.00	-0.88 -1.06	1.73 2.07	1.73 2.07	0.40 0.35	1.16 1.29

N- NORTH BRACE   ** - CROWN (N) CENTRE BRACE
S- SOUTH BRACE   * - SNCF & SCF AT CHORD CROWN (S)
C- CENTRE BRACE   (1) - SNCF   (2)- SCF

Table 3   Fatigue Response

Specimen		Applied Hot Spot Strain $\times 10^{-6}$	Applied Stress Ratio R	Crack Initiation $N_i \times 10^6$	Through Thickness Penetration $N_t \times 10^6$	Applied Cycles $N \times 10^6$	Cycles to Failure $N_f \times 10^6$	N_i/N_f %	N_t/N_f %
N° Type	Condition								
1 T	AW	±798	-1	0.1	1.5		2.55	3.9	58.8
2 T	SR	±790	-1	-	-	20	-	-	-
2 T	SR	±1570	-1	0.1	0.51		0.6	16.7	85
3 T	AW	±780	-1	0.4	1.12		1.55	25.8	72
4 T	AW	±763	-1	0.05	0.77		0.94	5.3	82
5 T	SR	±688	-1	2.5	8.29		9.07	27.6	91.4
6 T	AW	±805	-1	0.065	0.47		0.98	6.6	48
7 T	SR	±805	-1	0.34	1.03		3.3	10.3	31
8 TK	AW	+210-110	-0.52	-	-	5		-	-
		+613-102	-0.17	0.65	2.6		3.15	21	82.5
9 TK	SR	+210-110	-0.52	-	-	5	-	-	-
		+613-102	-0.17	-	-	3.5	-	-	-
		+903-22	-0.02	0.57	1.4		1.47	38.7	95.2

Typical Connection Elevation
Note: All Weld Toes to Become Tangent
to Pipe Surface Smooth Radius

1.5mm to 5mm
Root Opening

$\alpha = 75°$ 90°

Section"C-C"

1.5mm to 5mm
Root Opening

$\alpha = 90°$ 135°

45°
Min.

Section"B-B"

1.5mm to 5mm
Opening

$\alpha \leq 135°$

45° Min.

38mm

Section"A-A"

1.5mm to 5mm
Opening

$\alpha \leq 60°$

$\alpha/2$

Section"D-D"

For $t \leq 30mm$
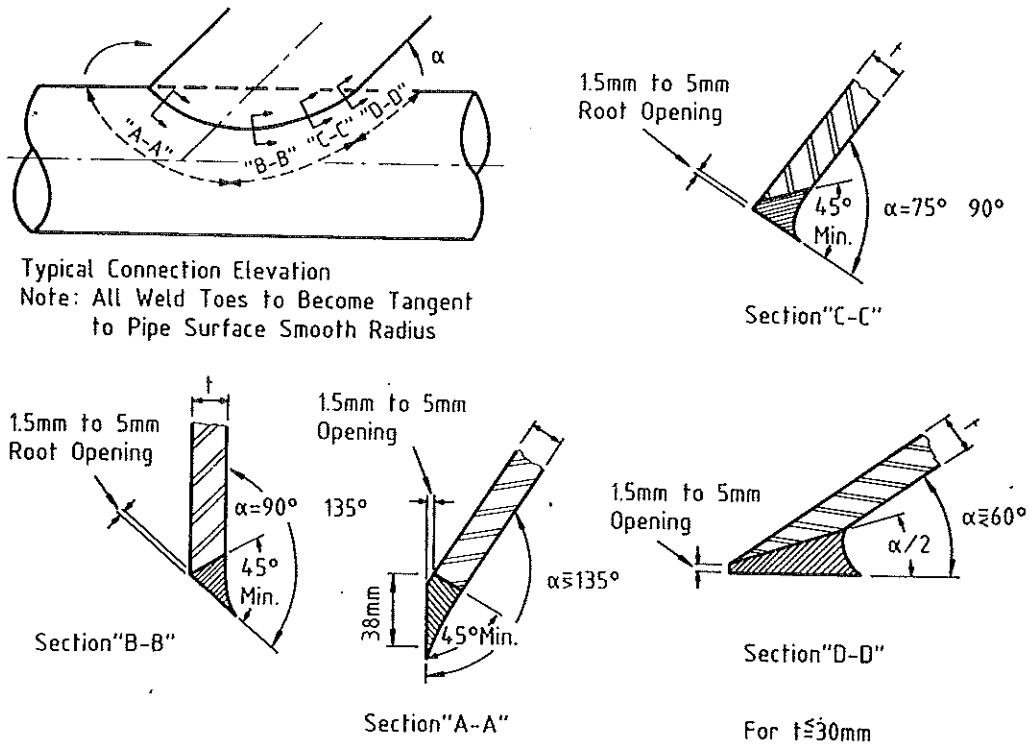
FIG.1 WELDED TUBULAR JOINT (After Wintermark, 2)

N.W   N   N.E

3.6% 5.9% 3.6%

12.3%   13.1%   8.5%

W   14.2% ← → 6.1%   E

16.1%   17.4%   12.3%

S.W   4.8%   7.8%   4.8%   S.E

S
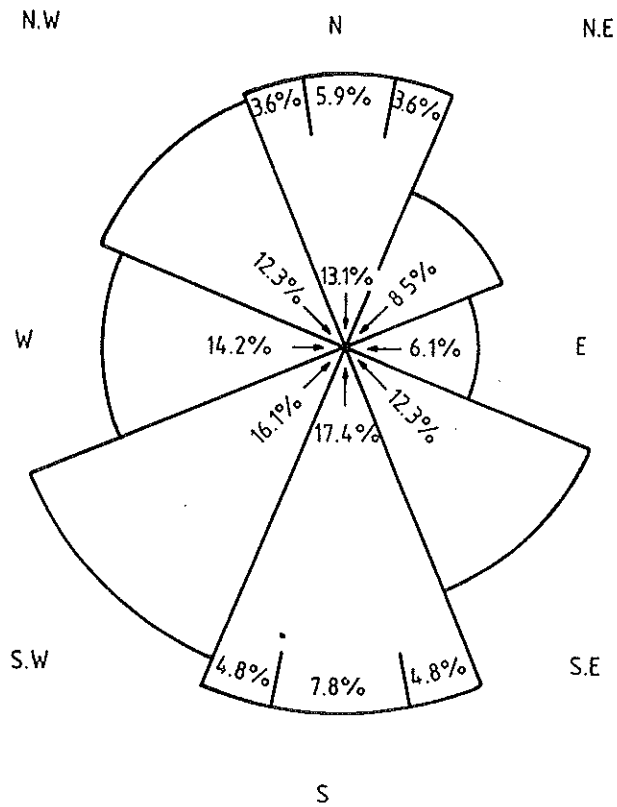
FIG.2 WAVE DIRECTION DISTRIBUTION AT NORTH SEA (After Zijp, 3)
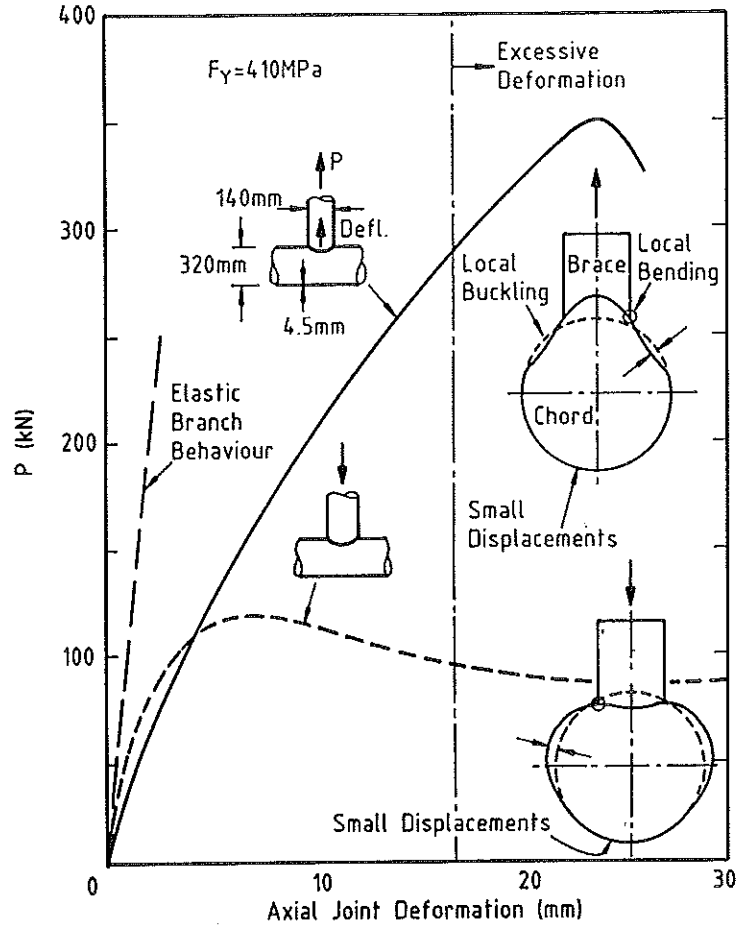
FIG.3 LOAD DEFLECTION BEHAVIOUR OF AXIALLY LOADED T JOINTS (4)
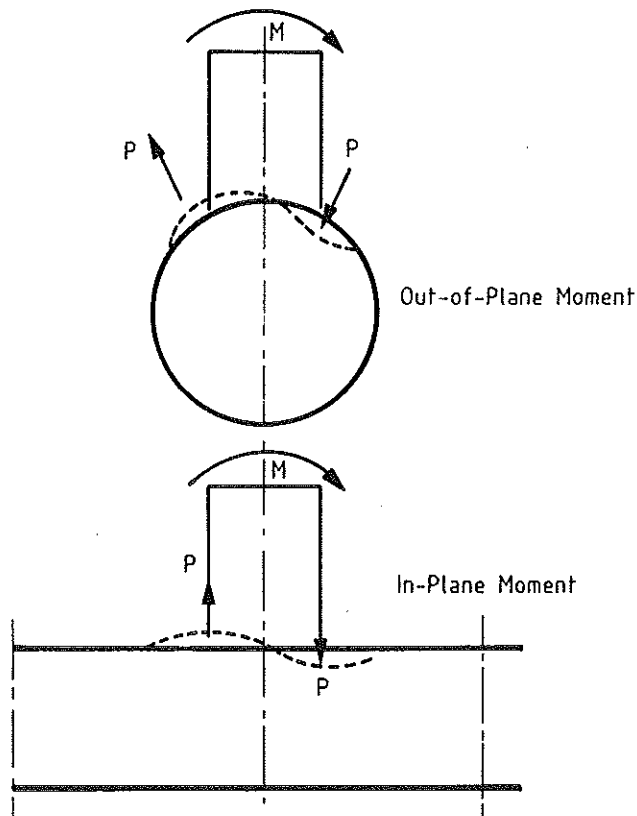
FIG.4 CHORD-WALL DEFORMATION DUE TO BENDING MOMENTS AT BRACE

Distance (mm)	Rosettes
100	2,3
50	4,5
12.5	6-13
12.5	14-25
50	26-29
100	30-32
150	33,34
200	35-37
250	38-39
300	40,41

SYMMETRICAL GAUGES

South   North

εⱠ./σⱠ.-Strain/Stress normal to weld toe
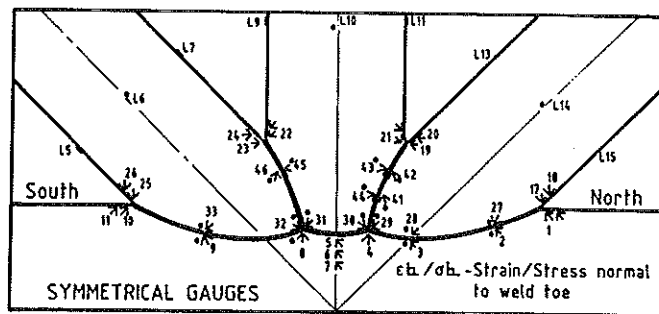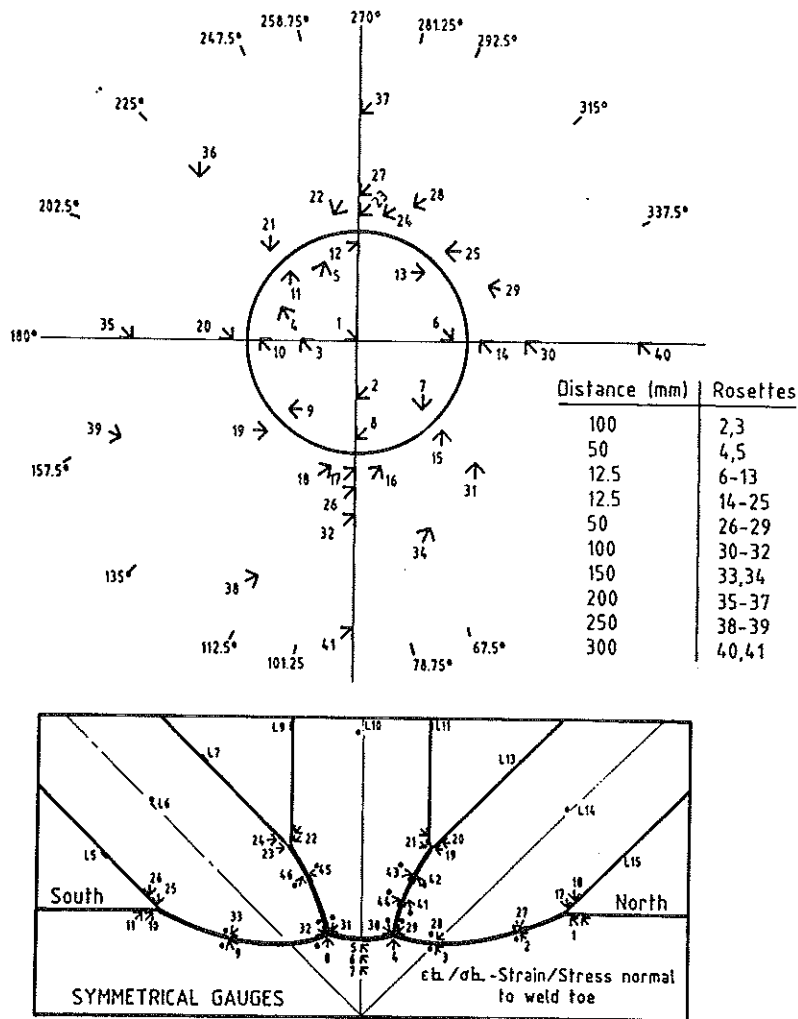
FIG.5   STRAIN GAUGE LOCATIONS ON OUTSIDE SURFACES
T AND TK SPECIMENS

FE Method

Curve Extrapolation

Linear Extrapolation

Brace

Strain Gauges
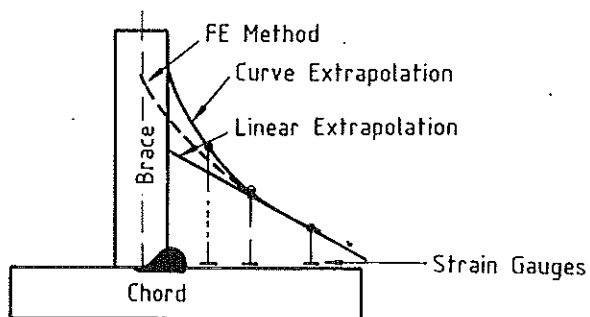
Chord

FIG.6   STRESS CONCENTRATION FACTOR DETERMINATIONS

0   D/4   D/2   3D/4   0
                                                      Nth.

0 — 1.2   1.3   1.8 2.3   1.7   1.4   1.3   0°
  -0.15   0.04   0.60 0.87   0.78   0.72   0.75

                      0.42 ⌐1.6

      1.5
 0.62   2.0   1.1 ⌐1.9

        1.3 ⌐1.9   1.2   0.47 ⌐1.2
  1.9   1.6 3.0
    2.3   0.25 ⌐0.85
 2.6 2.5   ⌐22.5°
 5.0 4.5 1.4   1 Unit Tensile
 1.3   1.9   0.05 ⌐0.72

 1.5
 0.47 -1.0   -0.32 ⌐0.24
       -0.12 ⌐-1.2
                                        45°
 -1.6
 -2.1   -0.85 ⌐-1.6

 π
 2
 -1.2
 -1.6

 90°   67.5°
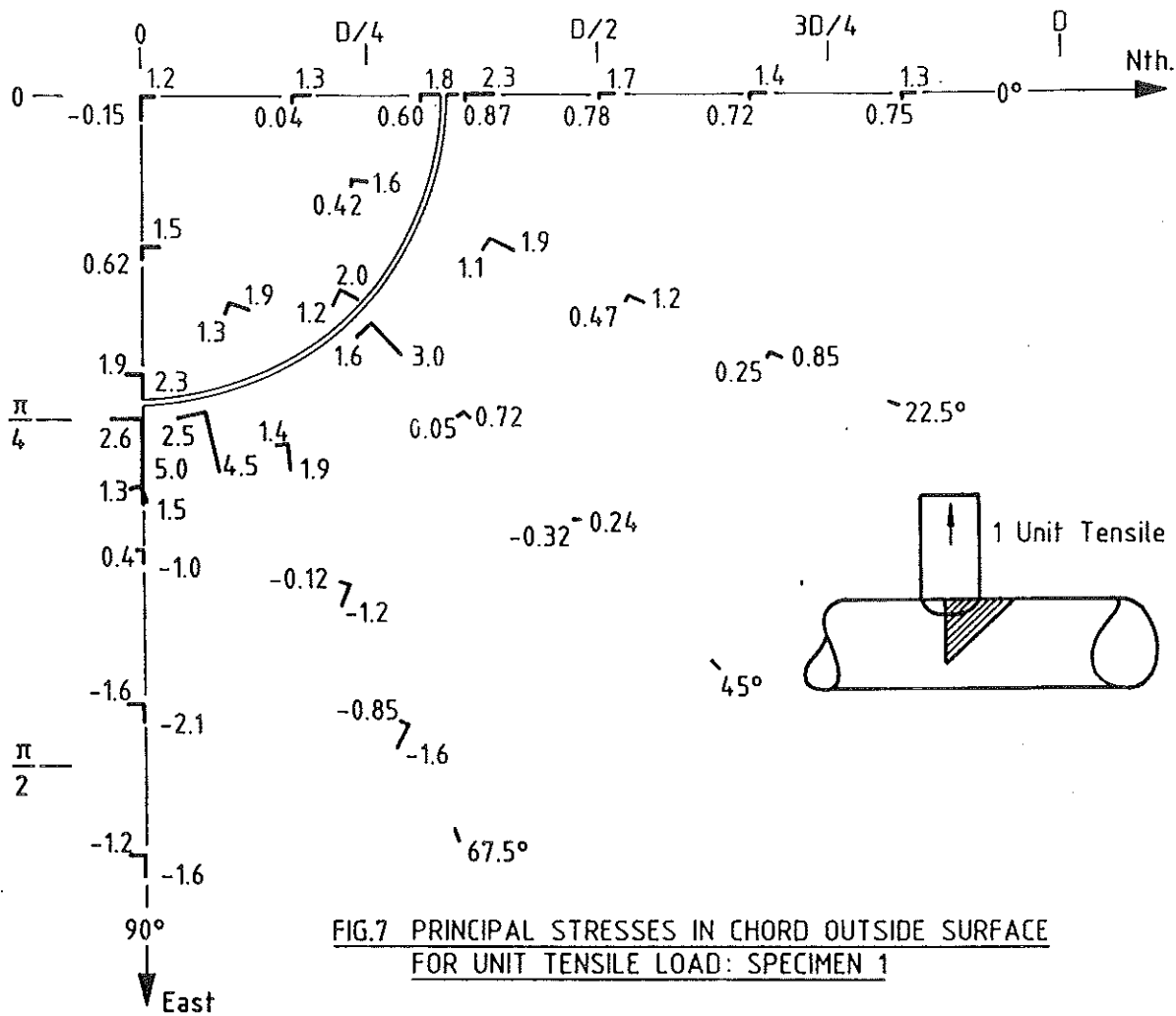
FIG.7 PRINCIPAL STRESSES IN CHORD OUTSIDE SURFACE
FOR UNIT TENSILE LOAD: SPECIMEN 1

East

5.86   3.67 1.42

1.67 ⌐

1.32 ⌐3.36   ⌐0.66 ⌐0.46
      4.65   6.57   5.35
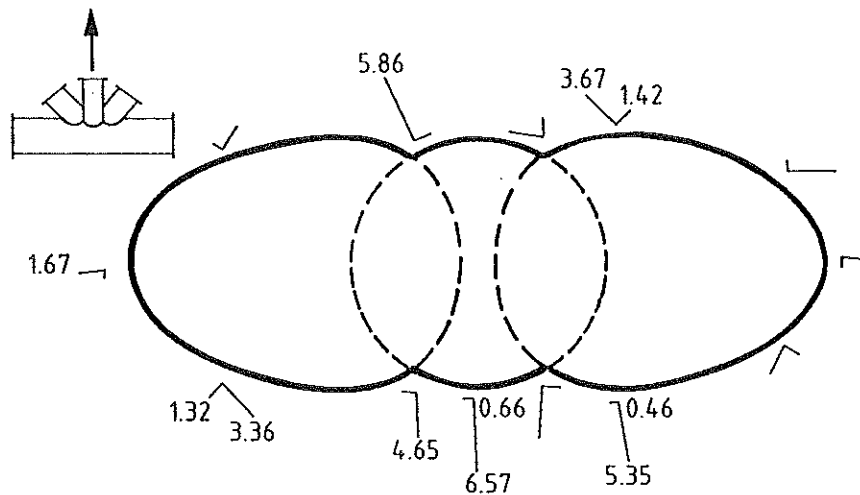
FIG.8 CHORD INSIDE PRINCIPAL STRESS UNDER
AXIAL LOADING ON THE C-BRACE

6.09

3.67

4.87

5.97

3.52

3.6

3.74

6.12
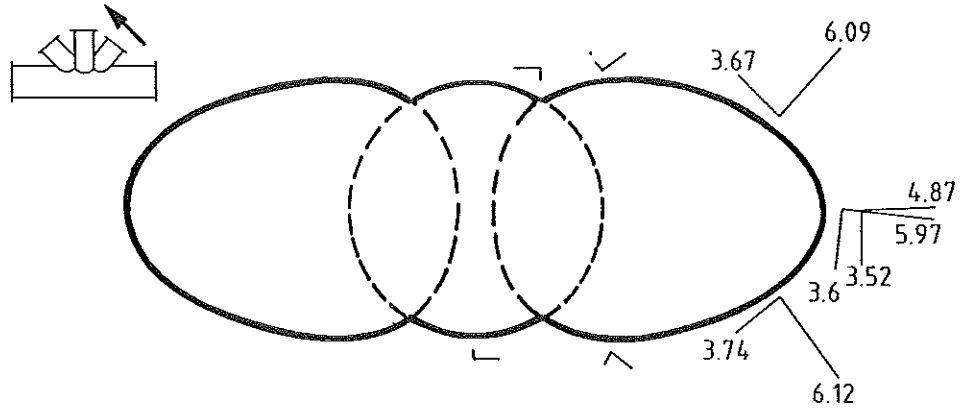
FIG.9 CHORD OUTSIDE PRINCIPAL STRESS FOR
IN-PLANE-BENDING ON THE N-BRACE

X

4.31

1.67

1.82
4.77

1.52

3.79

4.07
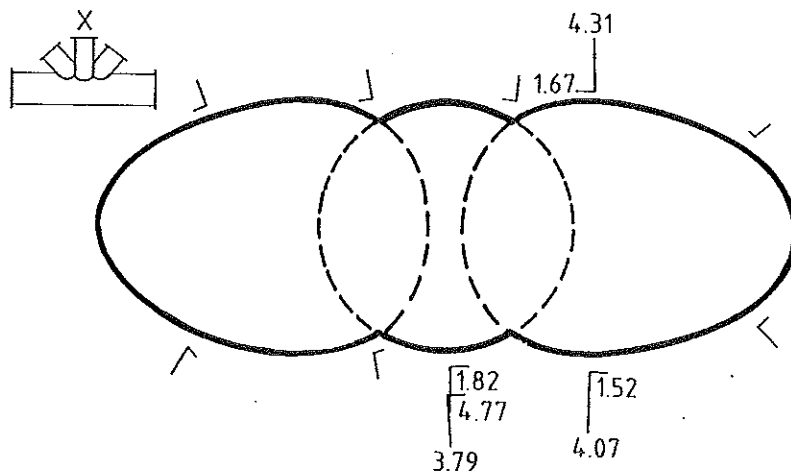
FIG.10 CHORD OUTSIDE PRINCIPAL STRESS UNDER
OUT-OF-PLANE BENDING ON THE C-BRACE
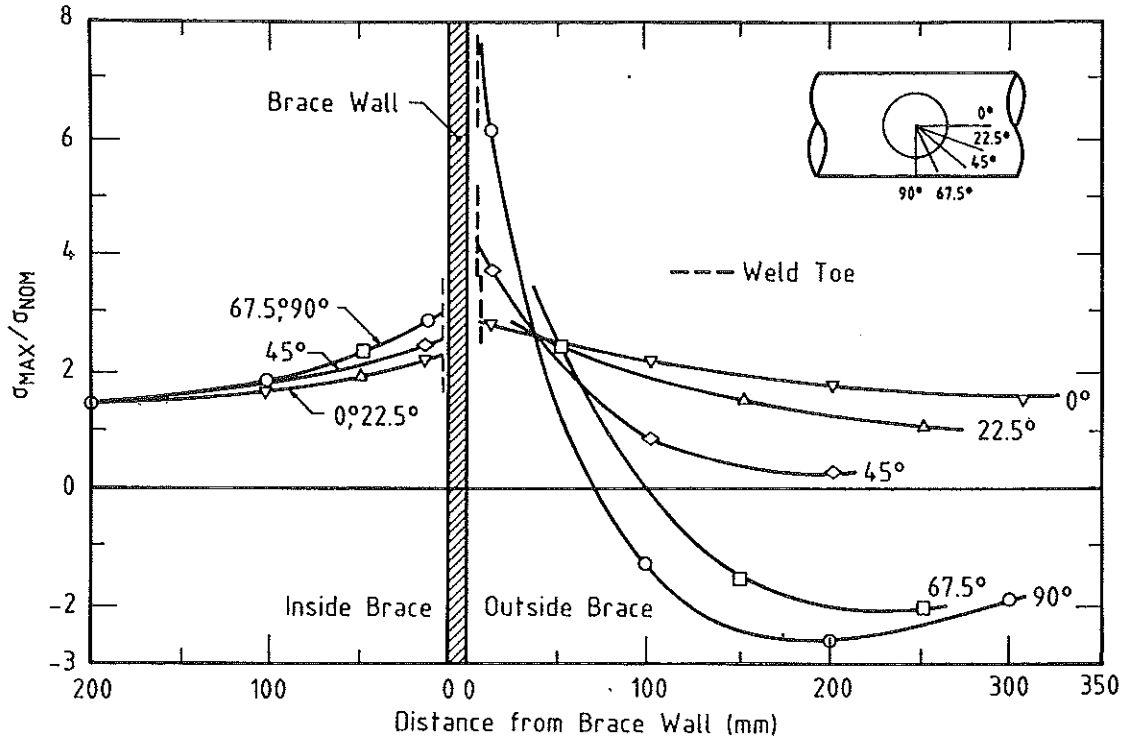
FIG.11   MAXIMUM STRESS IN CHORD OUTSIDE SURFACE: SPECIMEN 1
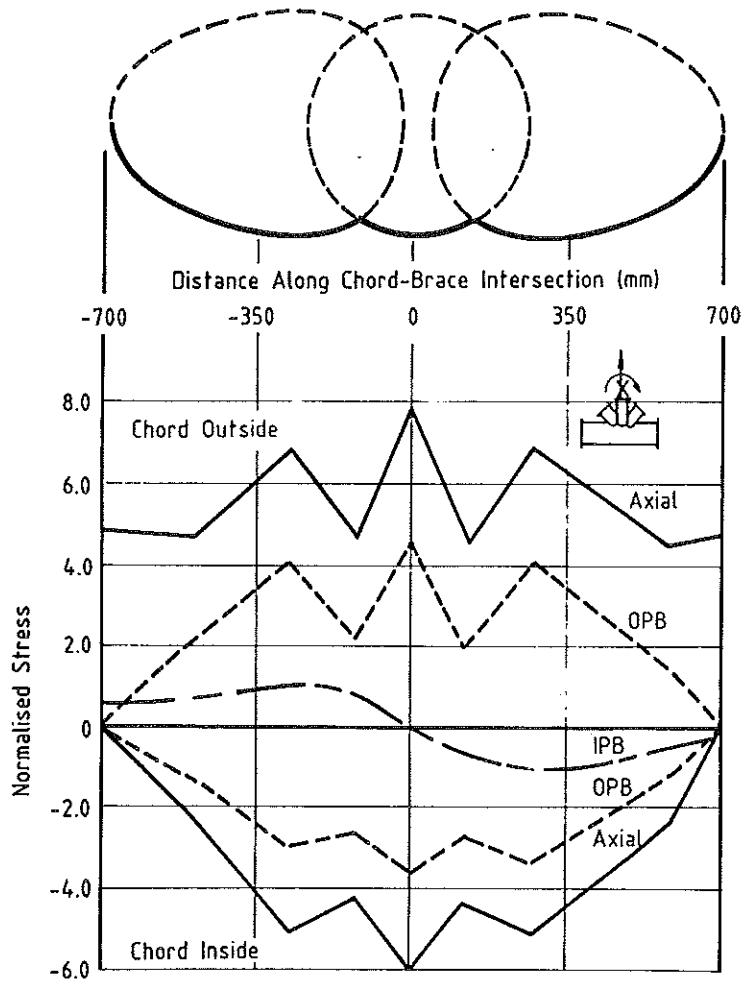
FIG.12   STRESS DISTRIBUTION ON CHORD OUTSIDE
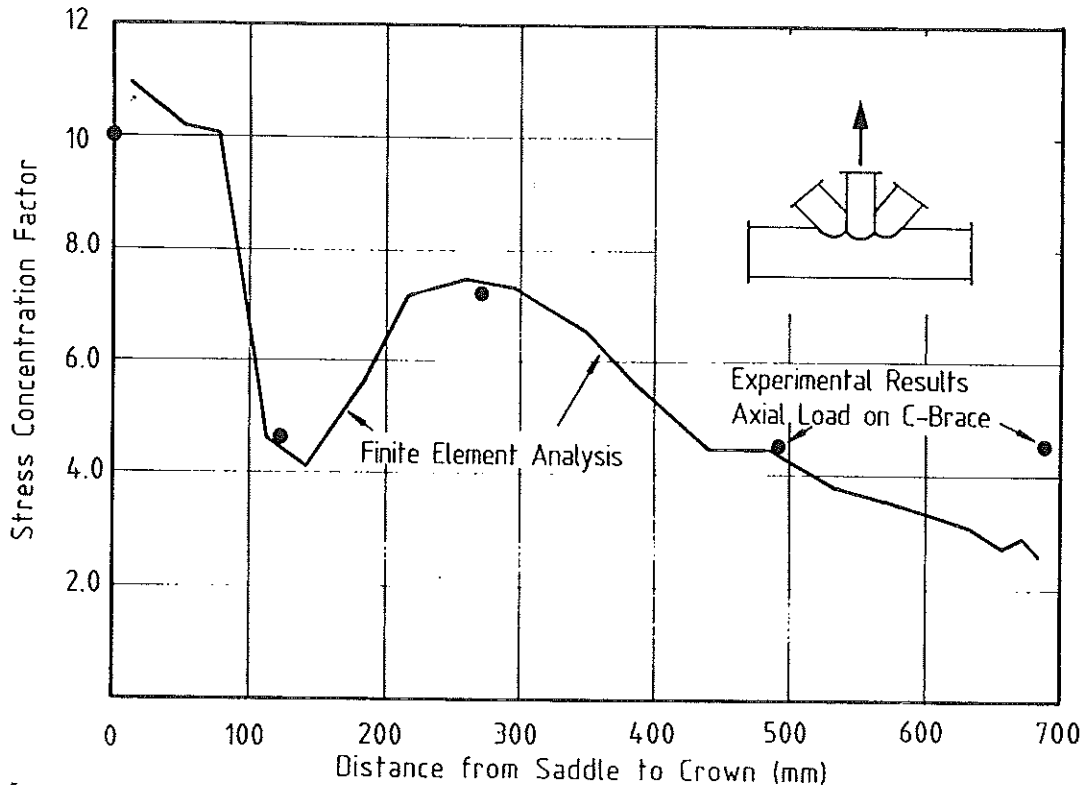AND INSIDE SURFACE
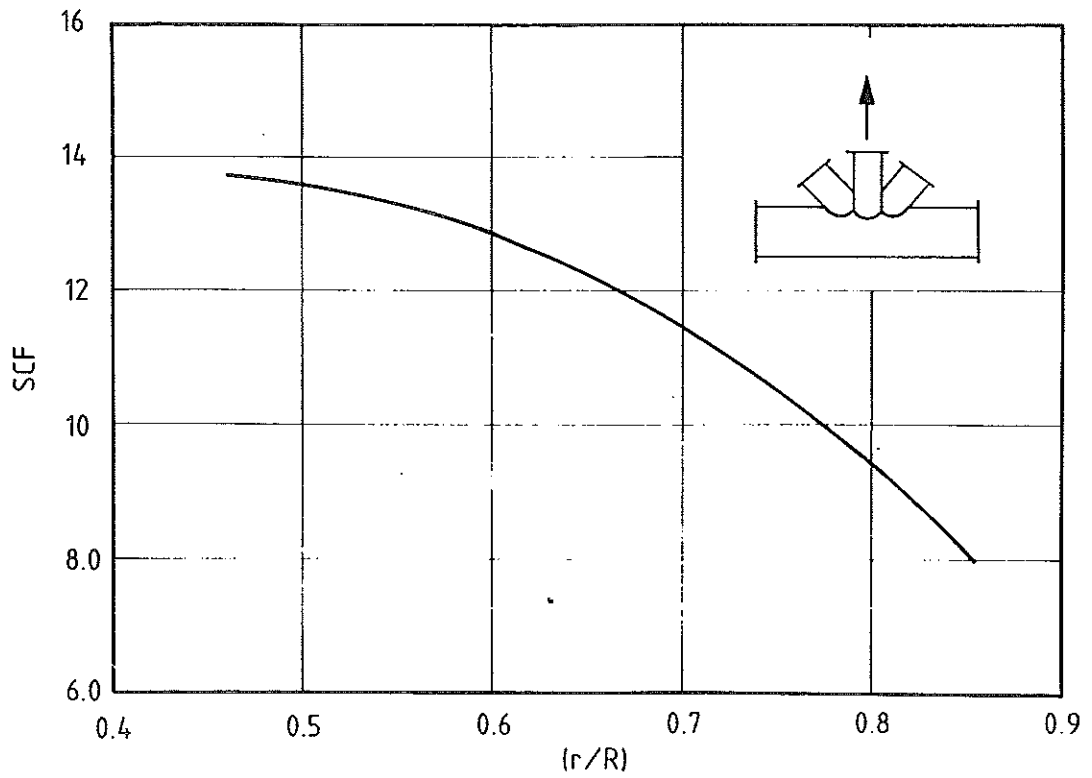
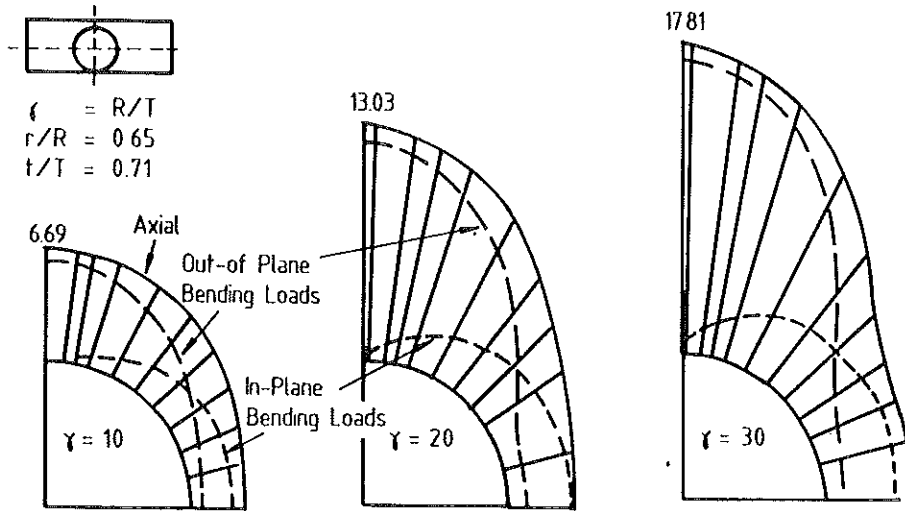FIG.13 STRESS DISTRIBUTION ON THE CHORD-BRACE INTERSECTION

FIG.14 INFLUENCE OF r/R ON THE SCF

FIG.15   THE INFLUENCE OF R/T ON THE PRINCIPAL STRESS DISTRIBUTION

Number of Cycles to Failure N_f
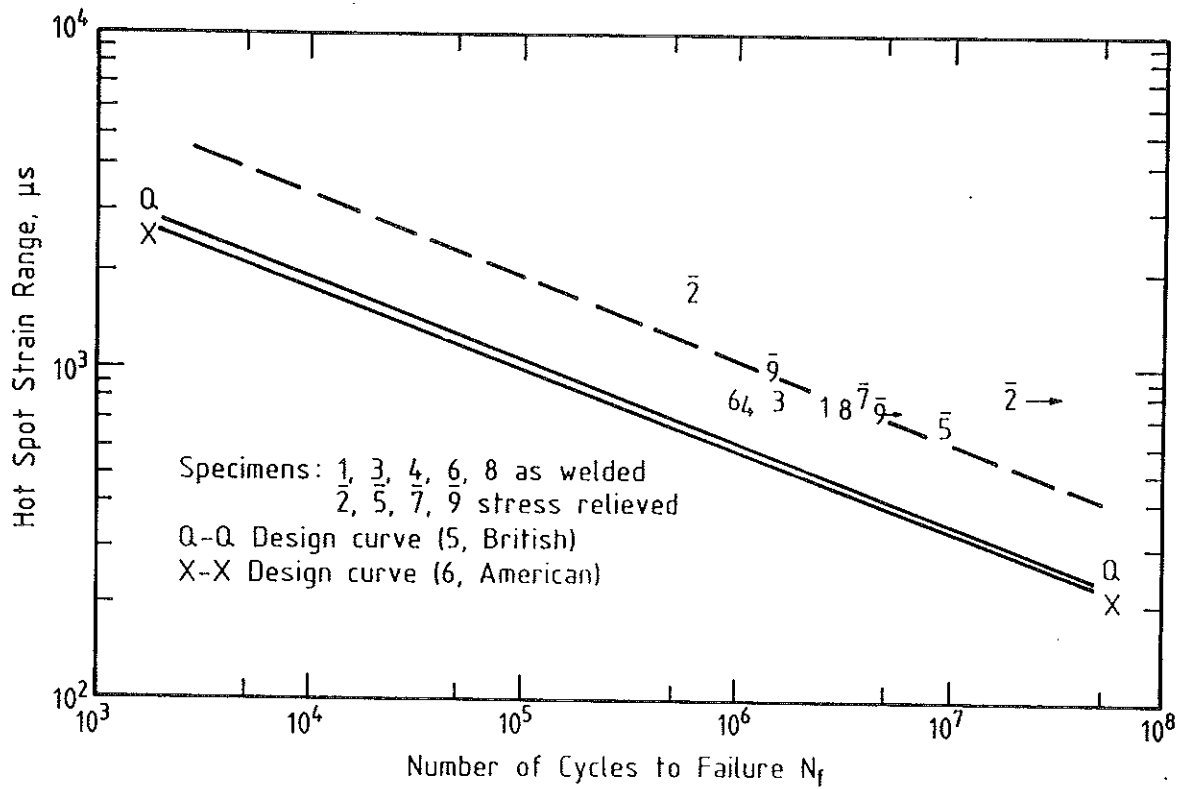
FIG.16   ASSESSMENT OF FATIGUE RESULTS
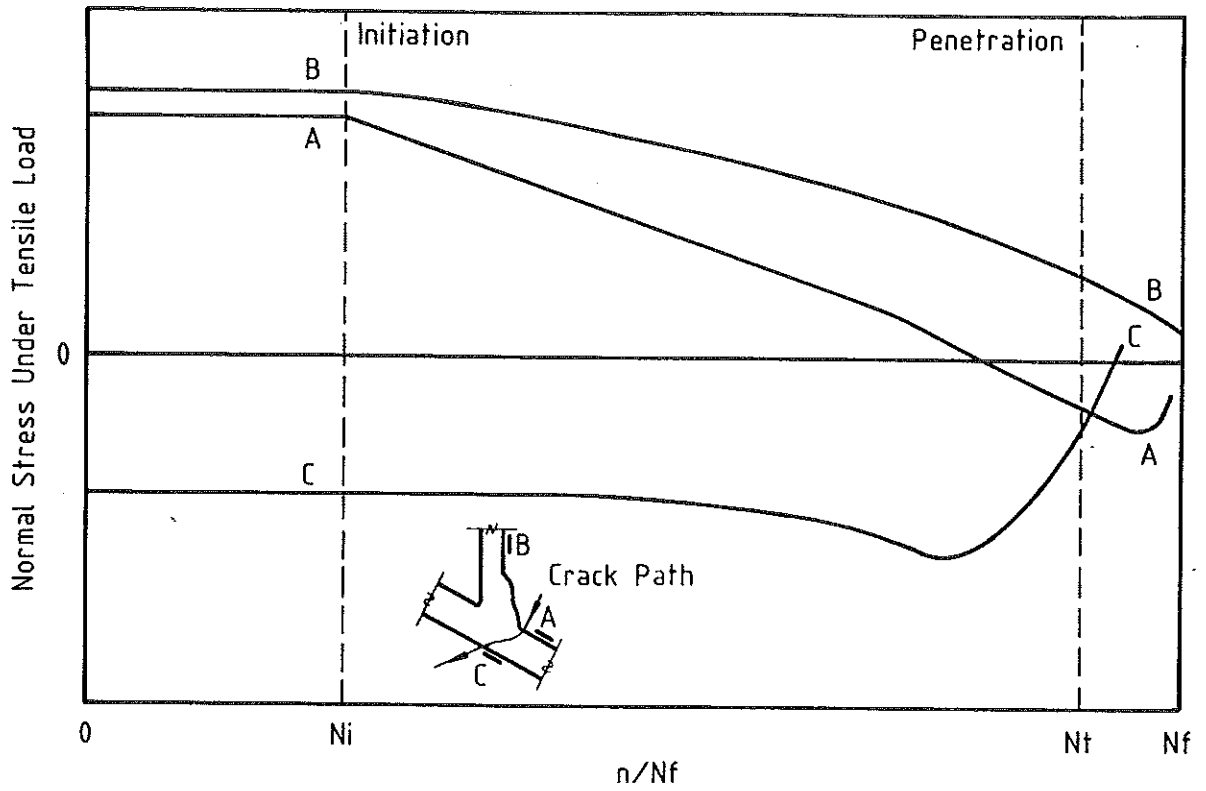
FIG.17 IDEALISED STRESS-CYCLE BEHAVIOUR AT
THE SADDLE: SPECIMEN 5
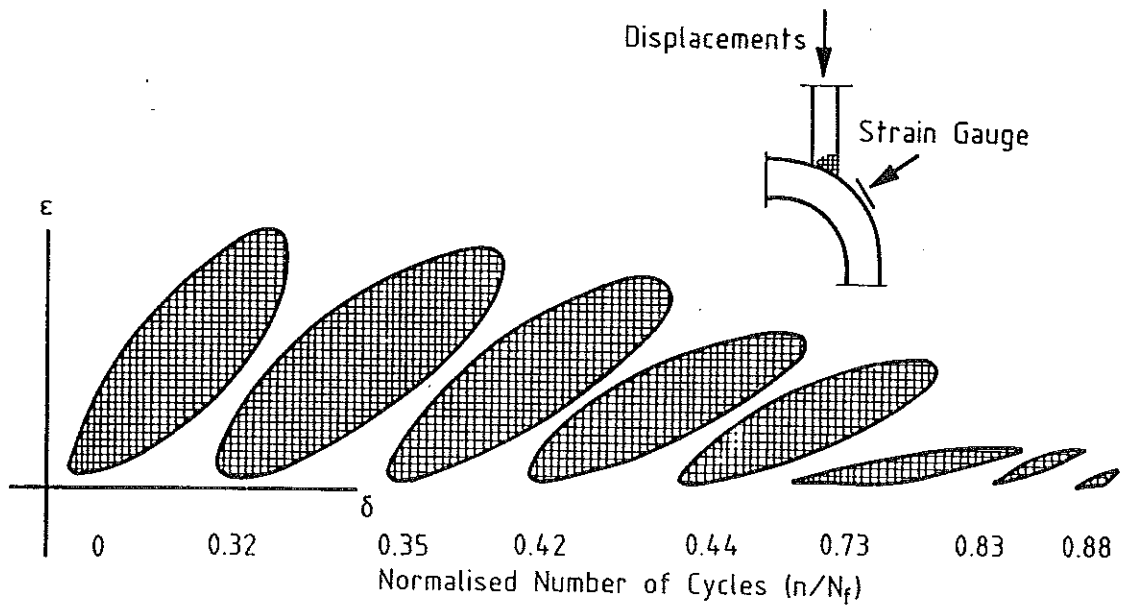
FIG.18 STRAIN-DISPLACEMENT HYSTERESIS LOOP DURING
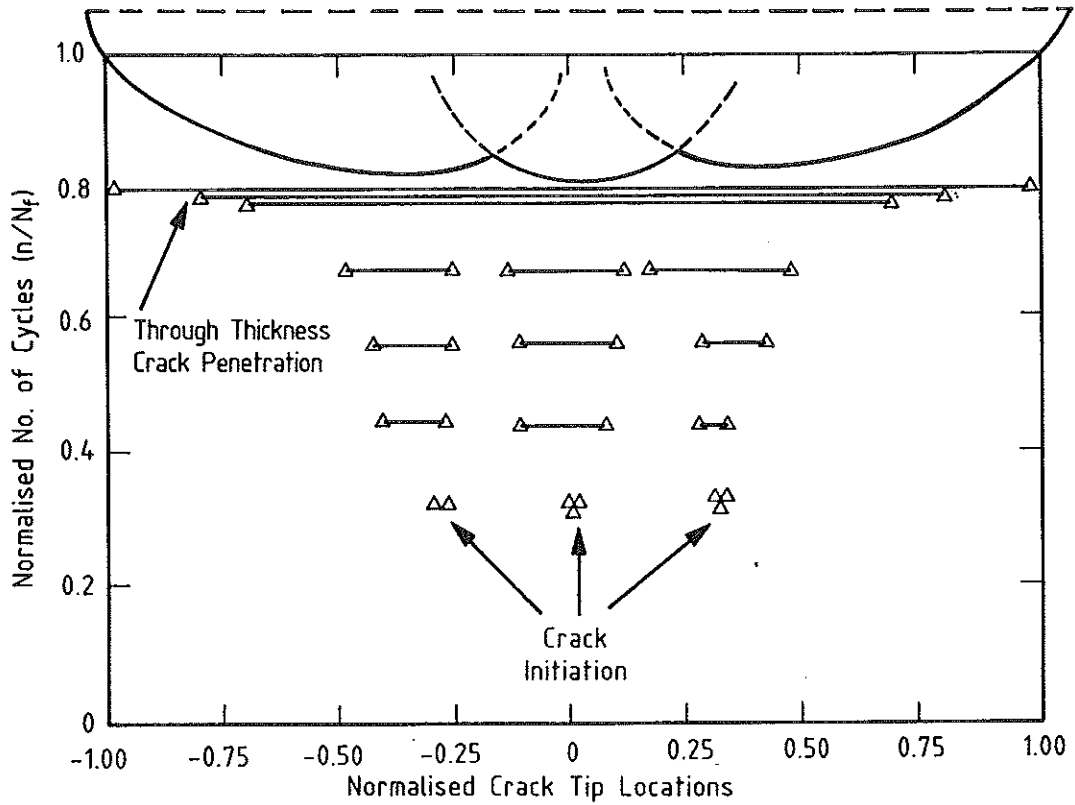CYCLIC LOADING FOR THE AW JOINT, SPECIMEN 8

FIG.19 EXTENT OF SURFACE CRACK DEVELOPMENT (SR)

Number	1	2	3	4	5	6	7	8	9	10	11	12	13
n/N_f	0.21	0.30	0.35	0.38	0.41	0.44	0.48	0.54	0.73	0.83	0.89	0.95	1.00

AS WELDED

STRESS RELIEVED
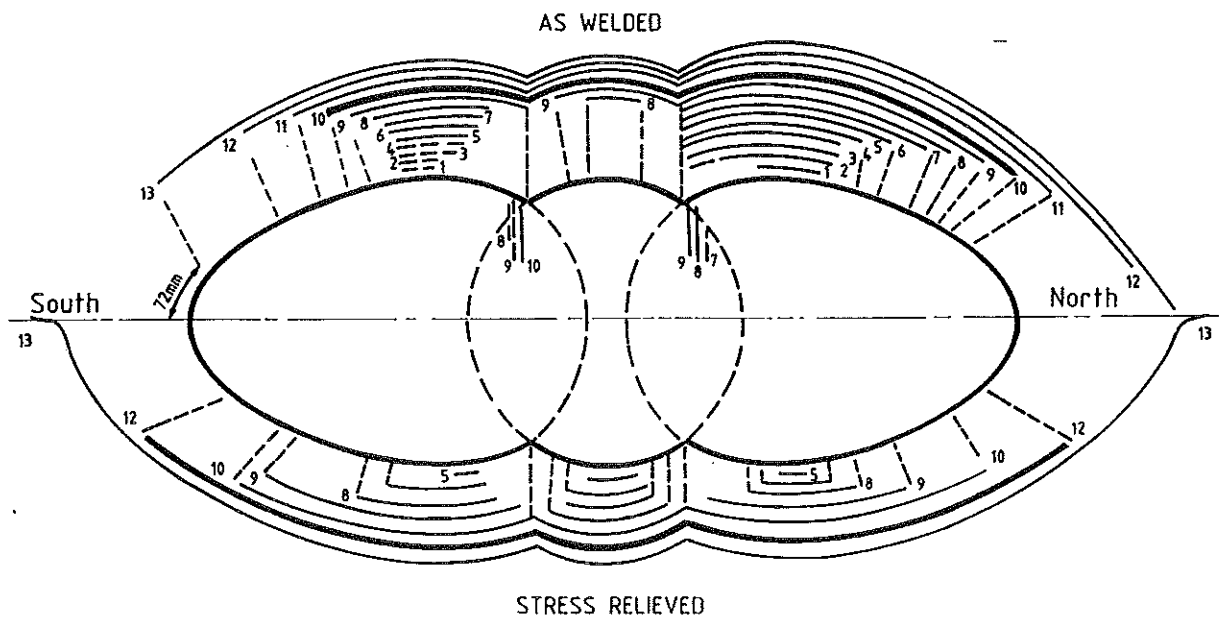
FIG.20 EXTENT OF SURFACE CRACK DEVELOPMENT
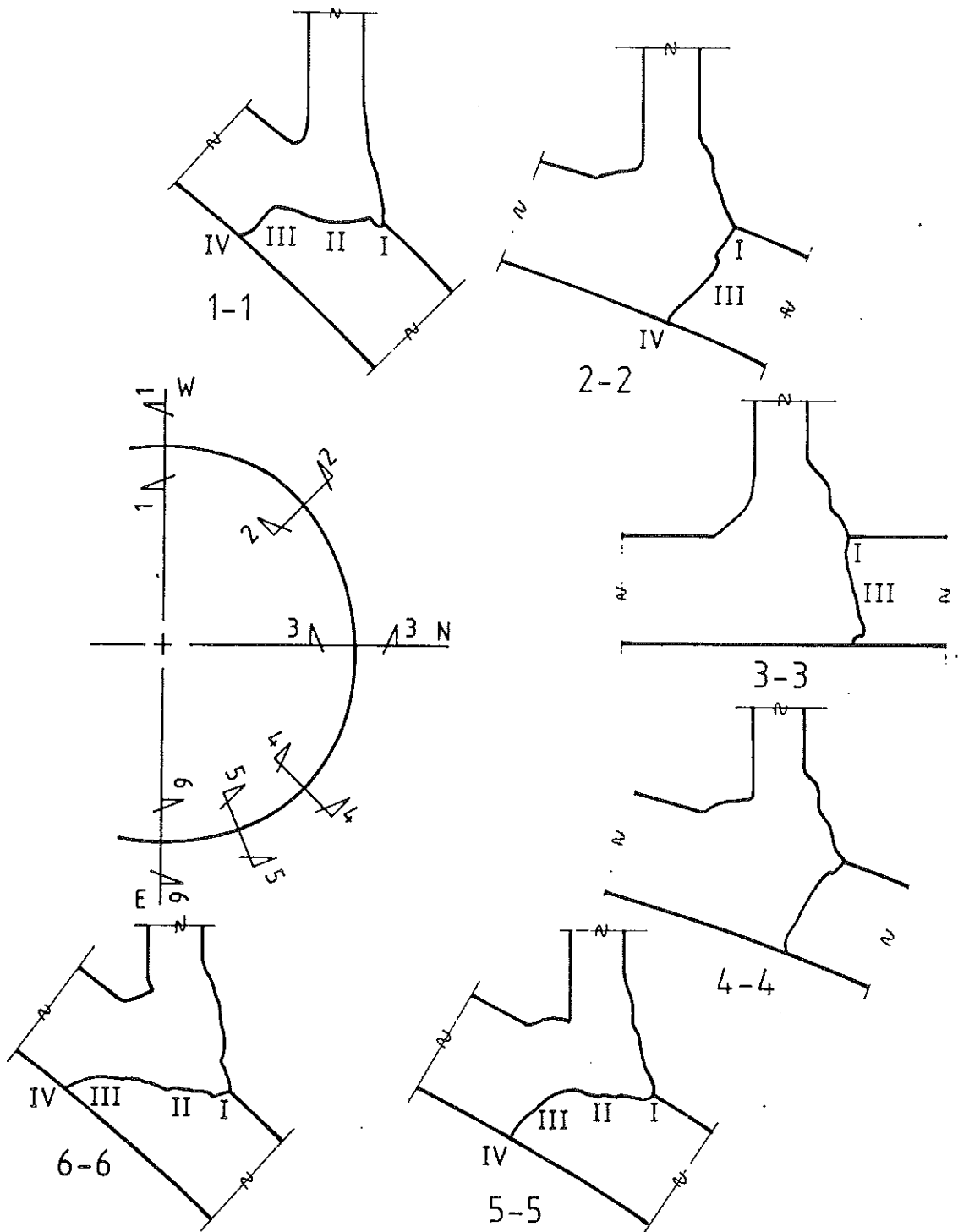
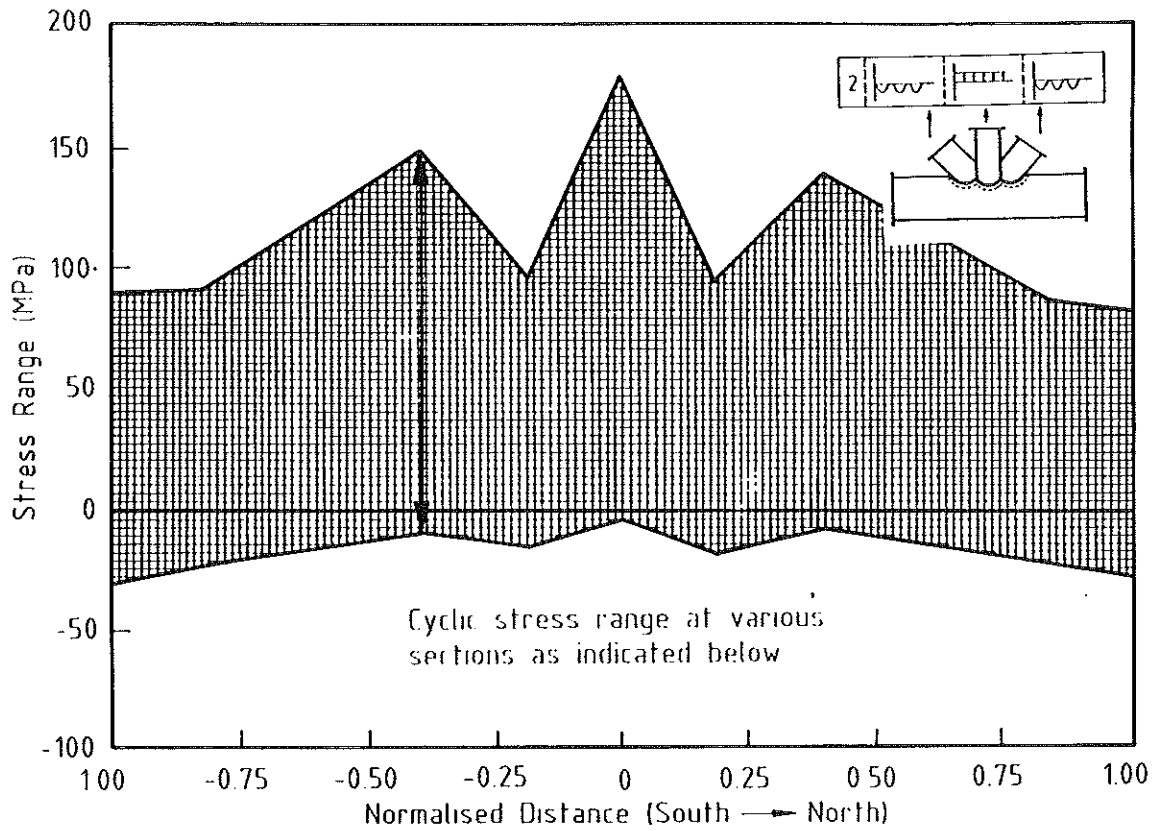FIG.21   THROUGH THICKNESS CRACK PATHS
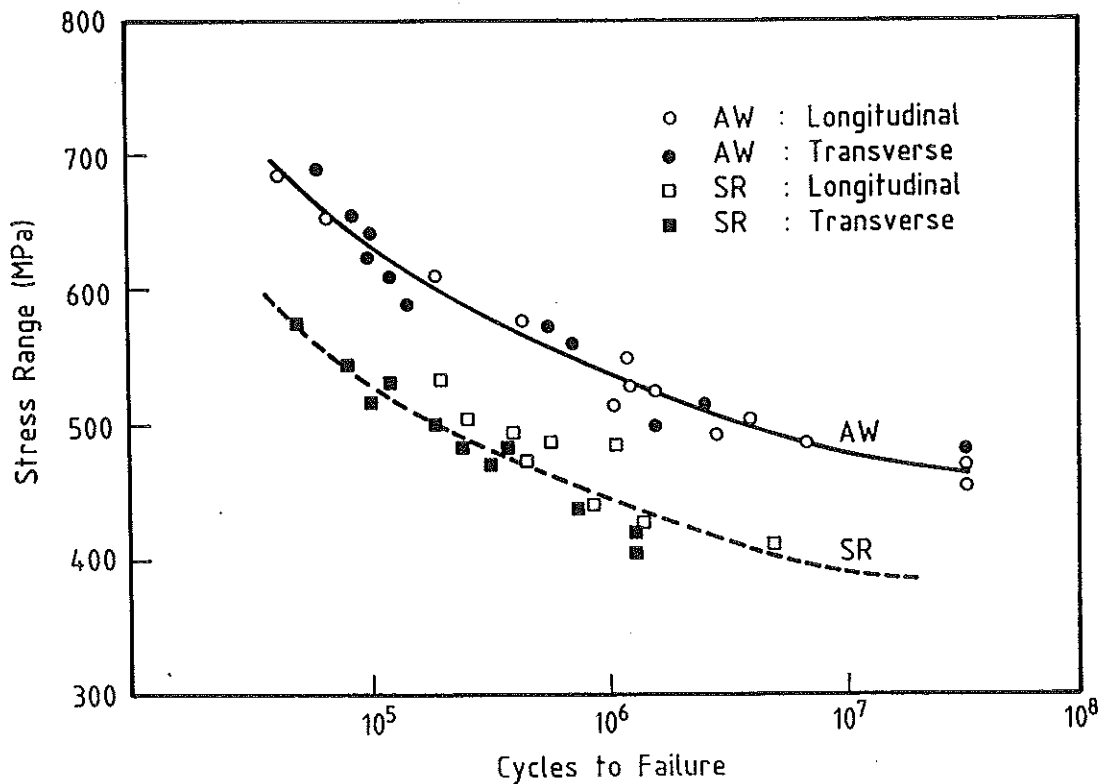SPECIMEN 1

FIG.22   CYCLIC STRESS PATTERN; PROGRAM 3

FIG.23   S-N CURVES FOR ROTATING BENDING TESTS
AB2525 MATERIAL, TK TYPE TUBULARS